Materials Research Proceedings 41 (2024) 1135-1143 https://doi.org/10.21741/9781644903131-125

Plasticity experiments on heavy gauge S700 steel

COPPIETERS Sam[1,a*], LAMBRUGHI Alessandro[1,b], VANCRAEYNEST Niels[1,c], ZHANG Yi[1,d], COOREMAN Steven[2,e] and STARMAN Bojan[1,3,f]

[1]KU Leuven, Department of Materials Engineering, Ghent Campus, 9000 Ghent, Belgium

[2]ArcelorMittal Global R&D Gent/OCAS NV, Ghent, Belgium

[3]University of Ljubljana, Faculty of Mechanical Engineering, Aškerčeva 6, 1000 Ljubljana, Slovenia

[a]sam.coppieters@kuleuven.be, [b]alessandro.lambrughi@kuleuven.be, [c]niels.vancraeynest@kuleuven.be, [d]yi.zhang@kuleuven.be, [e]steven.cooreman@arcelormittal.com, [f]bojan.starman@fs.uni-lj.si

Keywords: Heavy Gauge High Strength Steel, Plasticity, DIC, Delamination, IRT

Abstract. High Strength Steel grades are indispensable for the development of heavy-duty constructions and components with high specific strength. In these applications, a profound understanding of the plastic material behavior up to fracture is required to assess the structural integrity through numerical simulations. In this paper, we investigate the plastic behavior of S700 with a nominal thickness of 12 mm. The steel production process of a hot rolled, heavy gauge material inherently results in a through-thickness variation of the mechanical properties: i) solidification of the continuously cast slab starts from the outer surface, causing a gradient of the chemical composition across the thickness, ii) subsequent thermomechanical controlled rolling results in a variation of microstructure and texture over the thickness. To enhance the predictive accuracy of numerical simulations, we are examining the manifestation of this inhomogeneity across a range of plasticity experiments.

Introduction

The steelmaking process, involving multiple heating and cooling stages, leads to variations in chemical composition and microstructure across the thickness of high-strength steels. This inhomogeneity results in different grain sizes and structures in various parts of the steel, as demonstrated in studies like those by Raabe et al. [1]. Such variations can lead to direction-dependent mechanical properties, especially in the through-thickness direction, a phenomenon documented by numerous researchers. When the inhomogeneity is overlooked when simulating secondary forming processes such as bending, it can lead to inaccuracies in predicting the gradient of material properties throughout the material's thickness. Accurately characterizing the through-thickness variation of material behavior is crucial for creating precise simulations that are vital in assessing the structural integrity of heavy-duty components. Despite extensive research on the planar behavior of sheet metal, methods to evaluate through-thickness behavior are less developed. Through-thickness tensile tests on small samples from thick plates can provide insights, such as through-thickness ductility, but face limitations. These include dependency on plate thickness, the need to manufacture specimens without altering material behavior, and the requirement for suitable testing equipment. Techniques like welding extensions to small tensile specimens, as proposed by Barsom et al. [2], can alter mechanical properties due to the creation of a heat-affected zone. Moreover, such tests typically yield only the average through-thickness material behavior (i.e., across the gauge section of the small tensile sample) and do not provide detailed information on work hardening variation throughout the thickness. Furthermore, Barsom et al. [2] noted that through-thickness tests often reflect the properties of the weakest region across the thickness. In

contrast, the indentation hardness test is capable of detecting inhomogeneous material behavior in steel. However, despite their utility in estimating the initial yield stress, hardness measurements typically exhibit significant standard deviation. This substantial variability limits their effectiveness in accurately determining strain hardening behavior. A more direct method to assess work hardening variation through the thickness of steel is slicing a thick tensile specimen into thinner specimens for tensile testing, as suggested by Sohn et al. [3]. This method effectively provides the flow curve and material properties as a function of thickness, as shown in Section 1 of this paper. However, the use of this method is limited to analyzing pre-necking hardening behavior, only up to the point of maximum uniform tensile strain. Considering that secondary forming processes often induce strains that exceed this threshold, there arises a need for a methodology capable of determining the post-necking strain hardening behavior. Zhang et al. [4] introduced a Finite Element Model Updating (FEMU) technique to characterize the post-necking hardening behavior of thick, high-strength steel by exploiting the strain fields observed during diffuse necking in standard tensile tests. This method, however, operates under the assumption that material damage is negligible in the developing diffuse neck. As demonstrated in Section 2 of this paper, however, S700 steel is susceptible to delamination splits during diffuse necking, which compromises the applicability of Zhang et al.'s approach for this material. Consequently, as discussed in the third section of this paper, we utilize the free-end torsion test to ascertain the large strain flow curve of S700 steel.

Through-thickness strain hardening variation: the slicing method

An effective method for assessing work hardening behavior across the thickness of a material involves sectioning a thick tensile specimen into several thinner tensile specimens, as suggested by Sohn et al. [3]. The choice of sectioning method is critical to minimize its impact on the flow curve data. In this study, a 12 mm thick standard tensile specimen is sectioned using wire-cut Electrical Discharge Machining (EDM), a process that, despite its precision, unavoidably removes some material (wire diameter 0.31 mm) and partially releases residual stresses. Figure 1 illustrates the specimen being divided into eight distinct layers. It’s important to note that the outer layers (1 and 8, see Fig.1), with an average thickness of approximately 0.4 mm (as opposed to the 1.5 mm of the other layers), are excluded due to a significant thickness variability leading to heterogeneous strain fields before the maximum uniform tensile strain is reached. Consequently, only layers 2 to 7, which maintain consistent thickness, are used for reliable strain hardening analysis. Quasi-static tensile tests, with a nominal strain rate of $1.4 \cdot 10^{-4}$ s^{-1} in the gauge length of the specimen, are conducted using a standard tensile machine with a load-capacity of 250 kN. Stereo-DIC (Digital Image Correlation) is used to capture the strain fields on the surface of the specimens during the experiments. The DIC setup was configured with 6 MPx Manta G-609 cameras equipped with Kowa lenses (f=25 mm). The synchronization between the tensile load and the DIC system enabled to derive the strain hardening behavior. Fig. 2 presents the results, revealing significant differences in strain hardening behavior between layers 2 and 7 (labelled *sample 1.2* and *1.7*) and the more central layers 3 to 6. In general, symmetry around the sample's mid-plane is observed, with the corresponding layers (2 and 7, 3 and 6, 4 and 5) exhibiting similar strain hardening characteristics. Notably, the initial yield stress strongly increases towards the center of the specimen, with central layers 4 and 5 showing a distinct yield plateau, leading to Lüders bands visible in the measured strain fields. Additionally, Fig. 2 compares these results with those from a tensile test on the full thickness, indicated by the red triangles. Seemingly, the strain hardening behavior from the full thickness provides an averaged representation of the behaviors observed in the individual slices. For surface layers 1 and 8, which were not included in the direct measurement, it is assumed that their strain hardening behavior is analogous to that observed in the subsurface layers 2 and 7. The latter is verified by simulating the full-thickness tensile test accounting for the eight different layers. This simulation assumes that the surface layers (1 and 8) mirror the hardening behavior of

the subsurface layers (2 and 7), a hypothesis corroborated by the excellent match between the simulated and experimentally obtained strain hardening behaviors in Fig. 2. Finally, Table 1 enumerates the Young's modulus E, the initial yield stress σ_0, and the r-value r_0 of each layer. It can be observed that E and σ_0 are significantly higher in the central layers (4 and 5), while the r_0 exhibits minimal variation across the thickness. The final row of the table displays the results from the full thickness tensile test for comparison purposes.

Table 1. The variation of Young's modulus E, the initial yield stress $\boldsymbol{\sigma_0}$ and the r-value.

Experiment	***E* [GPa]**	***σ0* [MPa]**	***r₀* [-]**
Sliced specimens			
Sample 1.2	191	671	0.738
Sample 1.3	194	707	0.723
Sample 1.4	207	733	0.720
Sample 1.5	206	738	0.715
Sample 1.6	186	678	0.737
Sample 1.7	189	656	0.656
Average Slices	196	697	0.715
Std Dev Slices	8.64	31.08	0.0276
Full thickness	191	680	0.684

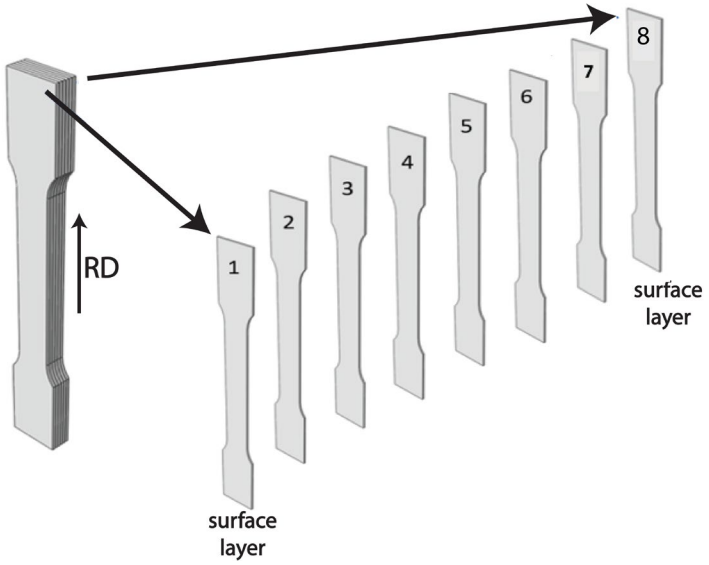

Figure 1. Slicing method: a full-thickness standard tensile specimen is sliced into 8 layers.

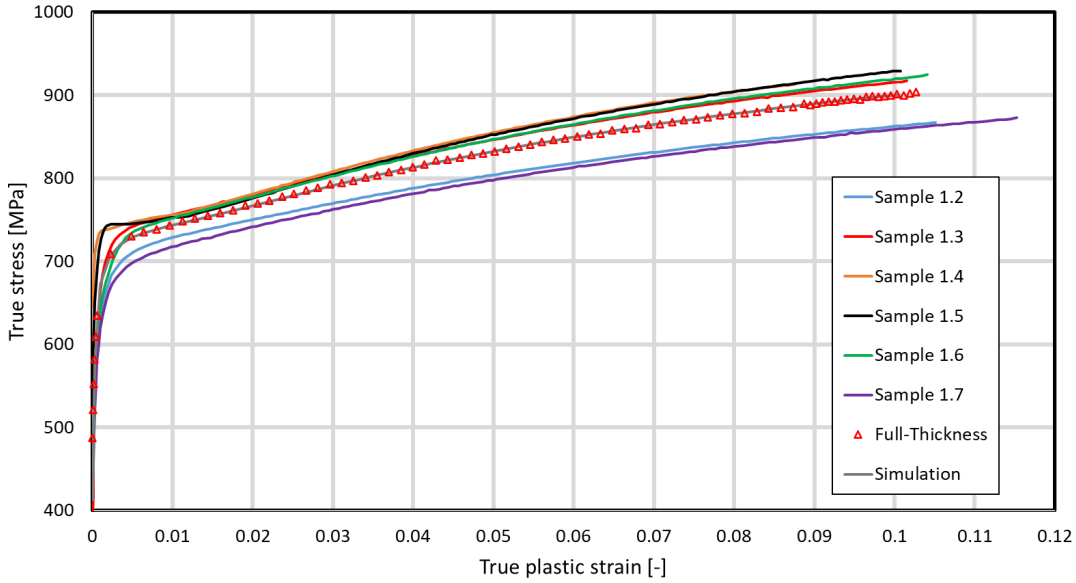

Figure 2. Variation in strain hardening behaviour (RD) through the thickness.

Occurrence of delamination splits during diffuse necking

A post-mortem inspection of a nonconventional tensile specimen, fractured under a quasi-static strain rate, revealed delamination splits in the 12 mm thick S700 steel [5]. Delamination refers to the material's splitting along its rolling plane when under tension, a phenomenon that notably affects the material's upper shelf energy and transition temperature. Influenced by various factors such as the steel grade, segregation of impurity atoms, and spatial variations in material strength, this issue is particularly evident in S700 steel, as demonstrated in the previous section. To provide a more comprehensive understanding of delamination in thick S700 steel, we performed tensile tests (in the rolling direction) at different nominal strain rates, continuing the experiments until fracture with a constant cross head speed ($1.3\frac{mm}{min}, 58\frac{mm}{min}$ *and* $288\frac{mm}{min}$). The tensile tests were performed on a standard tensile machine with a load capacity of 250kN with hydraulic grips. For temperature assessment, we employed a Long-Waves (LW) infrared thermographic camera (FLIR 615A) equipped with a 24.6 mm lens to measure the local surface temperature of the specimen. The samples, painted black with white speckles, facilitated simultaneous accurate measurement of full-field thermal and kinematic fields. The emissivity of this paint was considered constant and equal to $\varepsilon = 0.93$ [-] as characterized by Cholewa et al. [6]. The latter assumption was verified by comparing the measurements from Infrared Thermography (IRT) and a thermocouple. Local strains were measured using a stereo-DIC setup. The integration of IRT into the stereo-DIC system ensured that the local temperature was available for each DIC data point. Flir BlackFly cameras (5MPx) with Kowa lenses (f=25 mm) were used. Each speckle pattern had an average speckle size of approximately 5px. A performance analysis was conducted to determine the most optimal DIC settings for each experiment. The maximum strain noise floor in the experiments was 323 μStrain. Using the optimal DIC settings, the thermal noise floor was estimated from still images under thermal equilibrium [7] to an average noise level of 58 mK. A value being close to a Noise Equivalent Temperature Difference (NETD) of 50 mK reported by the camera's manufacturer.

Figure 3 illustrates the delaminations observed in the fractured specimens subjected to various strain rates. It is apparent from the figure that delaminations were more pronounced at lower strain rates and reduced with increasing strain rates. Specifically, a high density of delaminations is visible at the lowest strain rate, a central delamination at the medium strain rate, and an absence of delaminations at the highest rate. It is important to note that these occurrences of delaminations

were not discernible from the load-displacement curves. Furthermore, the load-displacement curves corresponding to different strain rates indicate that S700 steel exhibits strain rate independence. Figure 4 presents the strain and temperature fields on the surface of the specimen, measured using Digital Image Correlation (DIC) and Infrared Thermography (IRT). All the plots in Figure 4 correspond to a maximum total true axial strain of 0.63. Both strain and temperature fields share the same color bars on the right-hand side of the figure. It can be seen that for the smallest strain rate, the maximal surface temperature only reaches 42.6℃. For the mid and high strain rate, adiabatic conditions in the diffuse neck cause a significant temperature increase. Indeed, the mid and high strain rate yield a maximum surface temperature of 146℃ and 160℃, respectively. From the comparison between Fig. 3 and Fig. 4 it can be concluded that an increase in temperature corresponds to a reduction in delamination density. Before reaching the point of fracture, it is essential to highlight the rapid increase in strain rate, leading to adiabatic conditions and a corresponding temperature rise in the necking area. However, accurately measuring this phenomenon poses challenges due to its transient nature. Nevertheless, the current results clearly indicate that the delamination in S700 under tensile load is driven by temperature while the stress-strain response itself is rate independent.

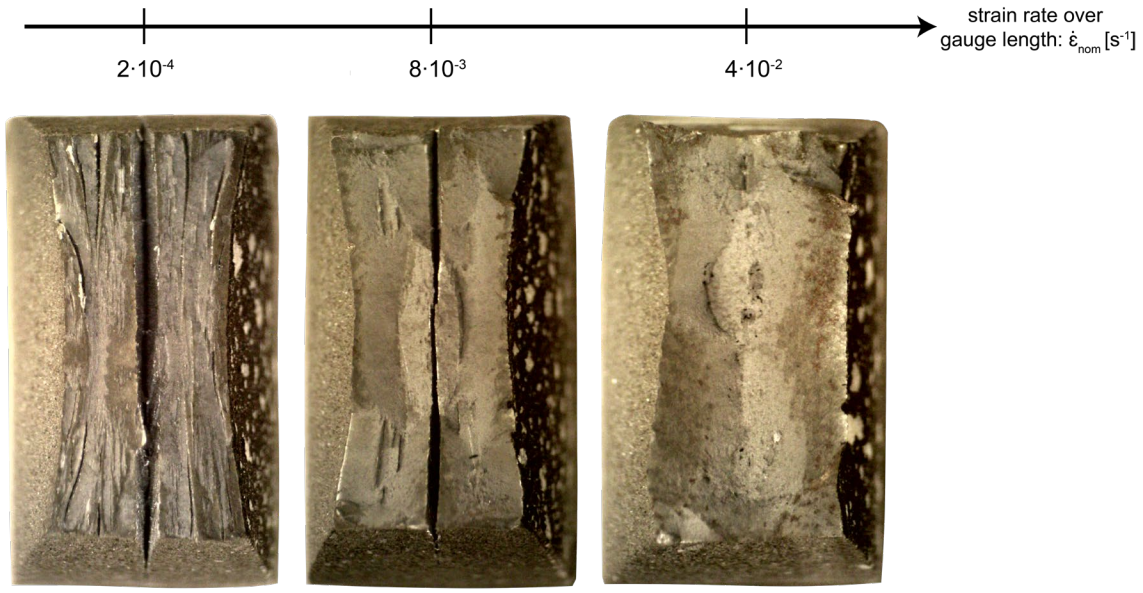

Figure 3. Delamination splits as a function of the nominal strain rate.

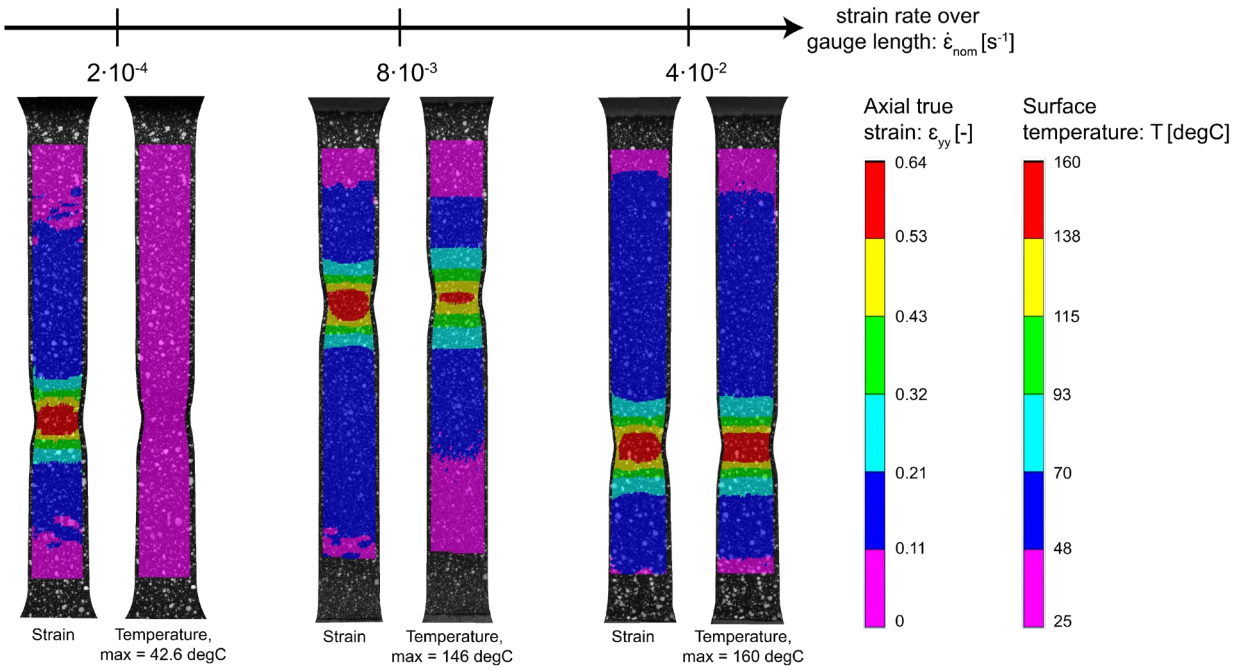

Figure 4. Axial true strain and surface temperature in the diffuse neck as a function of the nominal strain rate.

Large strain flow curve: the free-end torsion test

Figure 2 demonstrates that S700 steel reaches a maximum uniform tensile strain of approximately 0.1. However, beyond this point, S700 steel also shows a significant post-necking region extending up to fracture. To conduct accurate simulations for assessing the formability or structural integrity of S700 steel, it's essential to have data on its large strain flow curve. Zhang et al. [4] suggested an inverse method to extract this large strain flow curve from the diffuse necking observed in a tensile test. This method involves the use of Finite Element Model Updating (FEMU) and the analysis of measured strain fields. However, in the previous section is it shown that S700 exhibits delamination during diffuse necking which prevents the straightforward application of the FEMU approach to acquire the large strain flow curve. Vancraeynest et al. [8] proposed to use a free-end torsion test to inversely extract the post-necking hardening behavior of S700. The advantage is that in the free-end torsion test, large plastic strains can be probed without instability problems. More importantly, the delamination as observed in the tensile test does not occur in the torsion test. More details on the FEMU approach applied to the free-end torsion test can be found in [8].

To assess the robustness of the free-end torsion test in characterizing the large strain flow curve, three torsion samples (with a diameter of 8 mm) cut in the RD from a S700 steel plate were tested. The FEMU approach uses the torque-angle curve to identify the parameters of the selected hardening law. Vancraeynest et al. [8] recommended Voce's hardening law for describing the large strain flow curve of S700. An improved analysis (meshing strategy and explicit integration scheme), however, showed that Swift's hardening law is more appropriate than Voce in the probed strain range. The results of the identified Swift hardening laws are shown in Fig. 5. It can be inferred that the free-end torsion test enables to probe equivalent plastic strains up to 0.9. Despite the careful manufacturing of the specimens to ensure consistency in their through-thickness positions, some variation in the large strain flow curve is evident. The inset of Figure 5 displays a fractured specimen, where the torsion failure does not show a localized reduction of area. Notably, the plane of ductile shear failure is perpendicular to the longitudinal axis. It is evident from the inset of Figure 5 that the fractured parts are not perfectly aligned. This misalignment is attributed to the asymmetrical nature of ductile fracture. Furthermore, a post-mortem analysis of the fracture surface revealed no signs of delaminations. This observation is supported by Direct Current

Potential Drop (DCPD) measurements taken during the torsion tests. In the absence of pronounced necking in these tests, any change in the specimen's resistance directly correlates with the occurrence of delamination. Figure 6 indicates that the specimen's resistance during torsion remains approximately constant until fracture, thereby supporting the hypothesis that delamination is not a concern in the torsion test. This finding validates the use of the torsion test for reliably extracting the large strain flow curve. However, it's important to note that this identification assumes plastic isotropic material behavior, and the potential effects of plastic anisotropy warrant further investigation. Finally, it was observed that at a rotation angle of approximately 300°, the torsion sample begins to develop localized superficial spiral deformations.

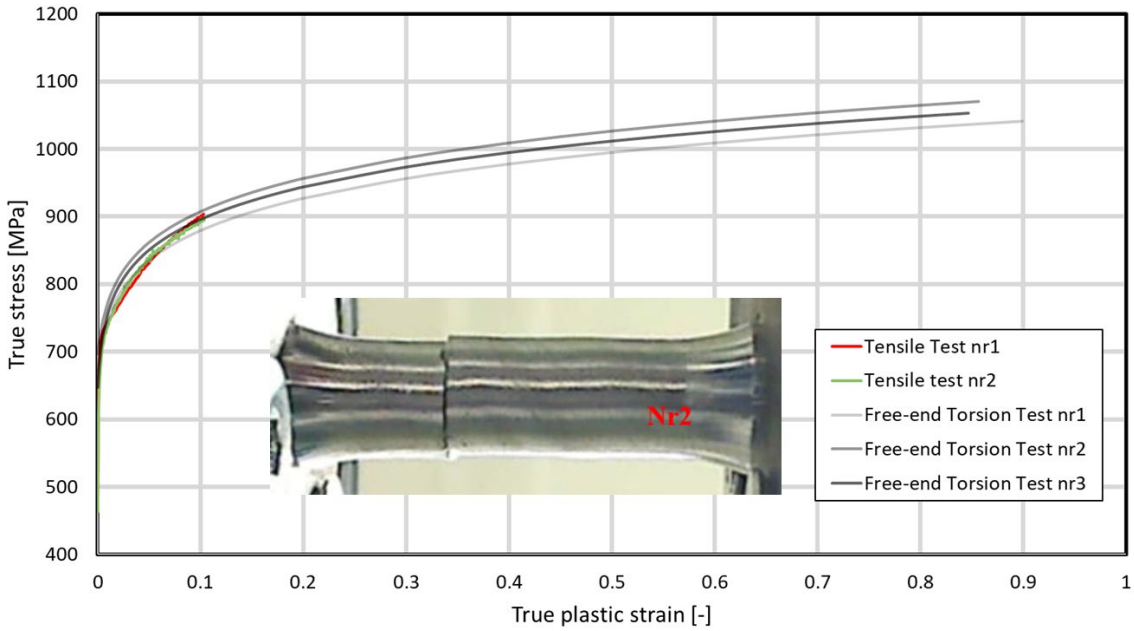

Figure 5. Strain hardening behavior identified through the free-end torsion test.

The spiral deformations previously mentioned are not clearly visible in the inset of Figure 5. To accurately determine their amplitude and frequency in the longitudinal direction of the torsion sample, which seems to be superficial, additional measurements were undertaken using the Atorn easyContour device equipped with a 120V/33 ceramic probe. This device boasts a maximum measuring range ($L_{z,max}$) of 30 mm and an error margin of $\pm 1.8\ \mu m + 2\left(\frac{L_z}{25}\right)$ in the z-direction. For aligning the torsion sample with the x-axis of the Atorn easyContour device, a V-block was employed. The orientation of the torsion samples in the V-block ensured that the principal material axis in the normal direction aligned with the z-axis of the measuring device. The results are presented in Figure 7. Despite meticulous efforts to align the torsion samples, the deformation patterns observed in tests 2 and 3 exhibit a slight skew. This skewness is attributable to the asymmetrical fracture behavior previously mentioned. At the point of fracture, the maximum amplitude of the spiral deformation is approximately 0.06 mm. The frequency of these deformations along the longitudinal direction of the torsion sample remains consistent across the three experiments. Further investigation is needed to understand the origin of this phenomenon and its potential impact on accurately identifying the large strain flow curve.

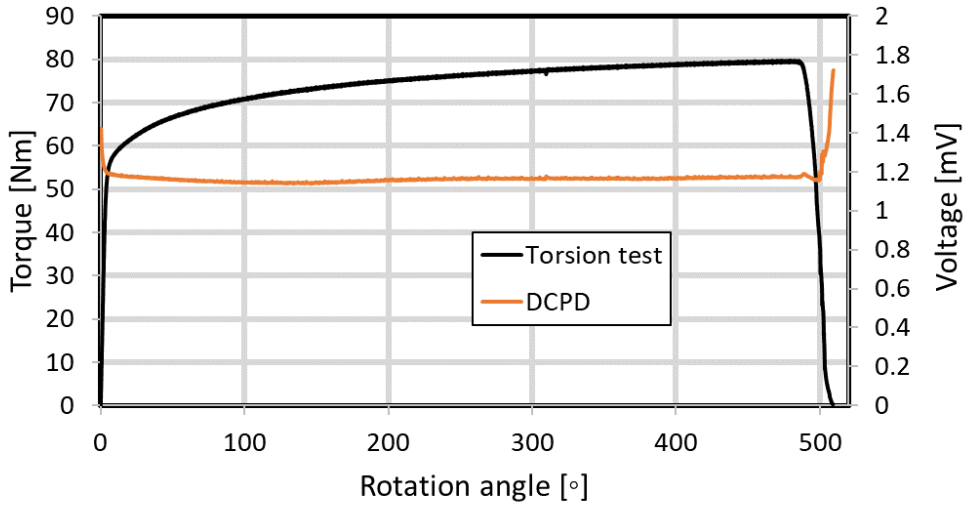

Figure 6. Direct Current Potential Drop (DCPD) measurement during the free-end torsion test.

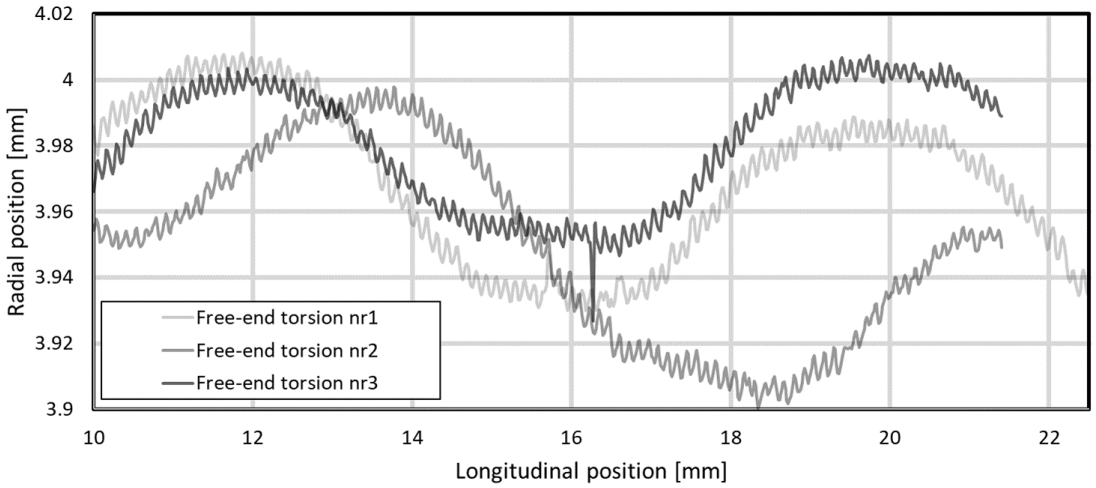

Figure 7. Superficial spiral deformation measured for three fractured torsion samples (S700)

Summary

From the experimental campaign on S700 steel, the following conclusions have been drawn:

- The slicing method distinctly reveals a through-thickness variation in the hardening behavior of the S700 steel in the rolling direction. Notably, the yield strength of the material increases significantly towards the mid-plane of the sample. However, there is no significant variation in the *r*-value observed.
- Tensile tests conducted at different strain rates on the full thickness of S700 steel indicate that its strain hardening behavior is strain rate independent. Nonetheless, temperature has been identified as the primary factor influencing the occurrence of delamination splits during diffuse necking under tension.
- The free-end torsion tests prove effective in probing large strains without inducing delamination splits at room temperature, making this method a viable option for extracting the large strain flow curve of S700 steel. Superficial spiral necking in the torsion sample

was noted at large rotation angles, a phenomenon that warrants further investigation in future studies.

Acknowledgement
The authors gratefully acknowledge the support from the Research Fund for Coal and Steel under grant agreement No 888153 (EU-RFCS 2019 project No. 888153 | vForm-xSteels).

Disclaimer
The results reflect only the authors' view, and the European Commission is not responsible for any use that may be made of the information it contains.

References

[1] Raabe D, Textures of strip cast and hot rolled ferritic and austenitic stainless steel.Mater. Sci. Tech. Ser. 11 (1995) 461–468. https://doi.org/10.1179/026708395790165192

[2] Barsom J, Korvink S, Through-thickness properties of structural steels, J. Struct. Eng. (1998) 727–735. https://doi.org/10.1061/(ASCE)0733-9445(1998)124:7(727)

[3] Sohn SS, Han SY, Bae J-H, Kim HS, Lee S, Effects of microstructure and pipe forming strain on yield strength before and after spiral pipe forming of api x70 and x80 linepipe steel sheets. Mat. Sci. Eng. A 573 (2013) 18–26. https://doi.org/10.1016/j.msea.2013.02.050

[4] Zhang H, Coppieters S, Jiménez-Peña C, Debruyne D, Inverse identification of the post-necking work hardening behaviour of thick HSS through full-field strain measurements during diffuse necking. Mechanics of Materials, 2019, 129 Pages 361-374. https://doi.org/10.1016/j.mechmat.2018.12.014

[5] Coppieters S, Zhang Y, Vancraeynest N, Lambrughi A, Cooreman S, Inverse Identification of a 3D Anisotropic Yield Function Through an Information-Rich Tensile Test and Multi-sDIC. Proceedings of the 14th International Conference on the Technology of Plasticity - Current Trends in the Technology of Plasticity. ICTP 2023. https://doi.org/10.1007/978-3-031-42093-1_66

[6] Cholewa N, Summers PT, Feih S, Mouritz AP, Lattimer BY, Case SW, A Technique for Coupled Thermomechanical Response Measurement Using Infrared Thermography and Digital Image Correlation (TDIC), Experimental Mechanics, Volume 56, 2016, Pages 145-164. https://doi.org/10.1007/s11340-015-0086-1

[7] Louche H, Analyse par thermographie infrarouge des effets dissipatifs de la localisation dans des aciers, thèse de doctorat, Université Montpellier II - Sciences et Techniques du Languedoc, 1999.

[8] Vancraeynest N, Cooreman S, Coppieters S, Identification of the large strain flow curve of high strength steel via the torsion test and FEMU. In: Material Forming – ESAFORM 2023: vol. 28, 1167-1174. https://doi.org/10.21741/9781644902479-127